INTERNATIONAL JOURNAL FOR NUMERICAL METHODS IN FLUIDS
Int. J. Numer. Meth. Fluids 2003; **41**:1137–1146 (DOI: 10.1002/fld.481)

Simulation of shockwave propagation with a thermal lattice Boltzmann model

ShiDe Feng[1,2,*,†], Ping Dong[2,‡], Michihisa Tsutahara[3] and Naoki Takada[3]

[1] *Laboratory of Numerical Modelling for Atmospheric Sciences and Geophysical Fluid Dynamics (LASG), Institute of Atmospheric Physics, Chinese Academy of Sciences, P.O. Box 9804, Beijing, China*
[2] *Division of Civil Engineering, Faculty of Science and Engineering, University of Dundee, Dundee DD1 4HN, U.K.*
[3] *Division of Industrial Science, Graduate School of Technology and Science, Kobe University, Japan*

SUMMARY

A two-dimensional 19-velocity (D2Q19) lattice Boltzmann model which satisfies the conservation laws governing the macroscopic and microscopic mass, momentum and energy with local equilibrium distribution order $O(u^4)$ rather than the usual $O(u^3)$ has been developed. This model is applied to simulate the reflection of shockwaves on the surface of a triangular obstacle. Good qualitative agreement between the numerical predictions and experimental measurements is obtained. As the model contains the higher-order terms in the local equilibrium distribution, it performs much better in terms of numerical accuracy and stability than the earlier 13-velocity models with the local equilibrium distribution accurate only up to the second order in the velocity u. Copyright © 2003 John Wiley & Sons, Ltd.

KEY WORDS: Lattice Boltzmann method; equilibrium distribution; shockwave

1. INTRODUCTION

In the last decade, there has been considerable progress in the development of lattice Boltzmann (LB) methods as novel alternatives to the traditional numerical methods (finite element, boundary element and finite difference) for solving the Navier–Stokes equations [1–3]. LB models have already found extensive applications in simulating the physical phenomena of various complexity ranging from flows in porous media [4], magnetohydrodynamics [5] immiscible fluids [6] to turbulence [7, 8].

* Correspondence to: ShiDe Feng, LASG, Institute of Atmospheric Physics, Chinese Academy of Sciences, P.O. Box 9804, Beijing, China.
† E-mail: fsd@lasg.iap.ac.cn
‡ E-mail: p.dong@dundee.ac.uk

Contract/grant sponsor: UK Engineering and Physical Sciences Research Council; contract/grant number: GR/R72532/01
Contract/grant sponsor: National Natural Science Foundation of China; contract/grant numbers: ZKCX2-SW-210 and 8-1502

Received October 2001
Revised 30 October 2002

As a common connection, it is well-known that the classic fluid dynamics equations such as Euler, Navier–Stokes and Burnett equations can all be obtained from the Boltzmann equation by a standard Chapman–Enskog expansion [2] retaining the zero-order, first-order and second-order terms in the series solutions, respectively. Also both numerical simulations and experimental verifications have shown that the Burnett equation perform better and are more generally applicable than the Navier–Stokes equation giving more accurate solutions for flows with a wider range of Kn numbers. This is because the higher-order approximation in deriving Burnett equation represents more closely the actual physical process of particle collision and movement. Unfortunately, the solution of the Boltzmann equation is extremely difficult and time consuming even in many physically simple situations [4] as the macroscopic fluids is the average result of Brownian movement of large number of microscopic particles. This computational difficulty severely restricts the application of the Boltzmann equation to real world fluid dynamics problems.

In contrast, the LB models solve the BGK-Boltzmann equation [4] by means of simple time and space discrete numerical methods involving a limited number of particles. This allows complex fluid dynamics problems found in practice to be solved efficiently. In a LB model, the population of particles moves in steps according to fixed set of deterministic rules. In most cases, these rules are chosen so that quantities such as particle number, momentum and energy are conserved in each collision. The transformation relation between the population of particles and macroscopic quantities is extremely simple involving no more than arithmetic calculations.

However, despite the progress made in developing the LB methods and its wide applications, the most existing lower-order LB models are found to be less successful in simulating supersonic flows. Although the simple shockwave-pipe can be reproduced satisfactorily using these models, simulation of the reflections of shockwaves on the surface of obstacles has met with considerable difficulties. Numerical instability and large artificial diffusion leading to unrealistically wide shock front are among the commonly known problems. In order to overcome these problems, a two-dimensional D2Q19 lattice Boltzmann model is developed in the present study based on the standard BGK-Boltzmann equation. This LB model strictly satisfies the conservation laws of mass, momentum and energy in collision process. Macroscopic fluid dynamic equations can be recovered using the standard Chapman–Enskog expansion retaining terms in the series solutions up to $O(u^4)$. The model is then used to simulate the reflection phenomena of shockwaves on the surface of obstacles. The preliminary numerical predictions were found to be consistent with that from the published experiment [9] and numerical instability problems associated with the lower-order LB models have been overcome.

2. LATTICE BOLTZMANN MODEL

The dynamics of a standard multi-speed LB system is usually represented by the BGK evolution equation for particle density:

$$f_{ki}(r_\alpha + c_{ki\alpha}\delta t, t + \delta t) - f_{ki}(r_\alpha, t) = \Omega_{ki} \tag{1}$$

with

$$\Omega_{ki} = \frac{1}{\tau}[f_{ki}^{(0)}(r_\alpha, t) - f_{ki}(r_\alpha, t)], \quad i = 0, 1, 2, \ldots, b; \quad k = 1, 2, 3, \ldots, n$$

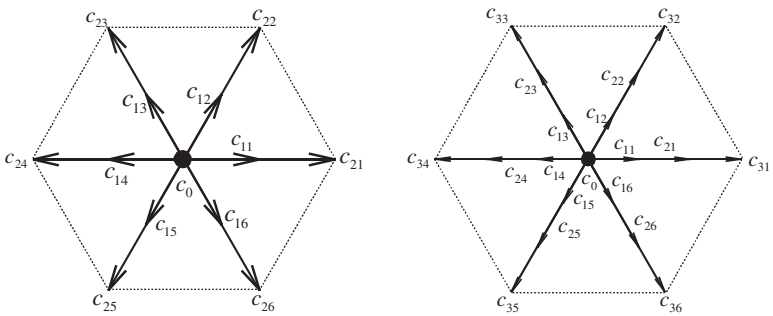

Figure 1. D2Q13 and D2Q19 model (Particle velocity $c_{2i} = 2c_{1i}, c_{3i} = 3c_{1i}$).

where f_{ki} is the distribution function of particle density, i is the number of movement directions of particles, n represents the number of particle speeds, $c_{ki\alpha}$ is the speed of the particle and it has the same modulus on all directions, $|c_{ki\alpha}| = c_k = \text{const}$ for $k = 1, 2, 3, \ldots, n$ with $c_{k0} = 0$, α represents co-ordinates index, δt is the discrete time step, Ω_{ki} is the collision operator, τ is the dimensionless relaxation time coefficient and $f_{ki}^{(0)}$ is the equilibrium velocity distribution function. In LB models, the choice of the equilibrium velocity distribution function is dependent on the discrete grids used. In this study, the hexagonal lattice as shown in Figure 1 is adopted. At each discrete site the particles will have three speeds for this D2Q19 model instead of only two speeds as in the case for a D2Q13 model. The mass, momentum and energy relationship criteria are satisfied through the following constraints that relate the microscopic particle populations and macroscopic fluid [2, 10]

$$\left[\rho, \rho u_\alpha, \frac{1}{2}\rho u^2 + \rho e\right]^{\mathrm{T}} = \begin{bmatrix} \sum_k \sum_i f_{ki} \\ \sum_k \sum_i f_{ki} c_{ki\alpha} \\ \frac{1}{2}\sum_k \sum_i f_{ki} c_k^2 \end{bmatrix} \tag{2}$$

In addition, the energy flux and momentum flux must also satisfy [2]

$$\left(\frac{1}{2}\rho u^2 + \rho e + P\right) u_\alpha = \frac{1}{2} \sum_k \sum_i f_{ki}^{(0)} c_k^2 c_{ki\alpha} \tag{3}$$

$$P\delta_{\alpha\beta} + \rho u_\alpha u_\beta = \sum_k \sum_i f_{ki}^{(0)} c_{ki\alpha} c_{ki\beta} \tag{4}$$

$$\delta_{\alpha\beta} = \begin{cases} 1, & \alpha = \beta \\ 0, & \alpha \neq \beta \end{cases}$$

where P is the pressure, ρ is the density of fluid and e is the internal energy of fluid per unit mass. The Chapman–Enskog expansion can be used to perform asymptotic expansion of the particle velocity distribution function in the neighbouring domain of local equilibrium

velocity distribution when the deviation of velocity distribution function f_{ki} from its equilibrium velocity distribution $f_{ki}^{(0)}$ is very small, which gives

$$f_{ki} = f_{ki}^{(0)} + f_{ki}^{\text{neq}} \tag{5}$$

$$f_{ki}^{\text{neq}} = f_{ki}^{(1)} + f_{ki}^{(2)} + \cdots + f_{ki}^{(n)} \tag{6}$$

$$f_{ki}^{(n)} = O(\varepsilon^{(n)}) \tag{7}$$

$$\partial^{(n)} f_{ki}^{(n)} = O(\varepsilon^{(n+1)}) \tag{8}$$

As the non-equilibrium distribution f_{ki}^{neq} has no contribution to density, momentum and energy [10, 11], i.e.

$$\sum_k \sum_i f_{ki}^{(\text{neq})} = 0 \tag{9}$$

$$\sum_k \sum_i f_{ki}^{(\text{neq})} c_{ki\alpha} = 0 \tag{10}$$

$$\sum_k \sum_i f_{ki}^{(\text{neq})} c_k^2 = 0 \tag{11}$$

the following conservation equations can be obtained from (2) using (9)–(11):

$$\left[\rho, \rho u_\alpha, \frac{1}{2}\rho u^2 + \rho e\right]^{\mathrm{T}} = \begin{bmatrix} \sum_k \sum_i f_{ki}^{(0)} \\ \sum_k \sum_i f_{ki}^{(0)} c_{ki\alpha} \\ \frac{1}{2} \sum_k \sum_i f_{ki}^{(0)} c_k^2 \end{bmatrix} \tag{12}$$

According to Reference [12], the following Maxwell distribution is adopted for the equilibrium velocity distribution function $f_{ki}^{(0)}$:

$$f_{ki}^{(0)} = W_k \rho \left(1 - 2E c_{ki\alpha} u_\alpha + 2E^2 c_{ki\alpha} c_{ki\beta} u_\alpha u_\beta + E u^2 - 2E^2 c_{ki\alpha} u_\alpha u^2 - \frac{4}{3} E^3 c_{ki\alpha} c_{ki\beta} c_{ki\chi} u_\alpha u_\beta u_\chi\right) \tag{13}$$

where W_k and E are constants that can be determined by the above conservation criteria. Substituting equilibrium distribution function (13) into criteria (3), (4) and (12) the weight W_k and coefficient E are obtained as shown in Table I.

Table I. Coefficients in the equilibrium distribution function.

D2Q13	D2Q19
$W_0 = 1 + \frac{2e^2(D+2) - 5Dec_1^2}{2Dc_1^4}$	$W_0 = 1 - \frac{4e^3(D+4)(D+2) + 49eD^2c_1^4 - 28e^2Dc_1^2(D+2)}{18D^2c_1^6}$
$W_1 = \frac{8Dec_1^2 - 4e^2(D+2)}{3bDc_1^4}$	$W_1 = \frac{2e^3(D+4)(D+2) + 18eD^2c_1^4 - 13e^2Dc_1^2(D+2)}{6bD^2c_1^6}$
$W_2 = \frac{2e^2(D+2) - Dec_1^2}{6bDc_1^4}$	$W_2 = \frac{20e^2Dc_1^2(D+2) - 4e^3(D+4)(D+2) - 9eD^2c_1^4}{30bD^2c_1^6}$
	$W_3 = \frac{2e^3(D+4)(D+2) + 2eD^2c_1^4 - 5e^2Dc_1^2(D+2)}{90bD^2c_1^6}$

Coefficients in both models: $E = -D/4e$, $P = (2/D)\rho e$, $D = 2$, $b = 6$, $c_3 = 3c_1$, $c_2 = 2c_1$, D is the number of spatial dimensions (2 in this case), b is the number of lattice direction (6 for the hexagonal lattice), W_0 and W_i are, respectively, the weights of stationary and moving particles.

3. FLUID DYNAMIC EQUATION

Macroscopically, the kinetic and thermodynamic behaviour of the fluid are governed by the fluid dynamic equations. Therefore, for an LB model to correctly represent the macroscopic fluid dynamics, it must be ensured that the fluid dynamic equations can be recovered from the LB models. Performing the usual Taylor expansion of the first term on the left-hand side of Equation (1) about time δt to the first and second order gives

$$\delta t : \frac{\partial f_{ki}}{\partial t} + c_{ki\alpha}\frac{\partial f_{ki}}{\partial r_\alpha} = -\frac{1}{\tau\delta t}[f_{ki} - f_{ki}^{(0)}] \tag{14}$$

$$\delta t^2 : \frac{\partial f_{ki}}{\partial t} + c_{ki\alpha}\frac{\partial f_{ki}}{\partial r_\alpha} + \frac{\delta t}{2}c_{ki\alpha}c_{ki\beta}\frac{\partial^2 f_{ki}}{\partial r_\alpha \partial r_\beta} + \delta t c_{ki\alpha}\frac{\partial^2 f_{ik}}{\partial t \partial r_\alpha} + \frac{\delta t}{2}\frac{\partial^2 f_{ki}}{\partial t^2} = -\frac{1}{\tau\delta t}[f_{ki} - f_{ki}^{(0)}] \tag{15}$$

Substituting the Chapman–Enskog expansion of the velocity distribution function Equations (5)–(8) into the above equations gives

$$\varepsilon : \frac{\partial f_{ki}^{(0)}}{\partial t} + c_{ki\alpha}\frac{\partial f_{ki}^{(0)}}{\partial r_\alpha} = -\frac{1}{\tau\delta t}f_{ki}^{\mathrm{neq}} \tag{16}$$

$$\varepsilon^2 : \frac{\partial f_{ki}^{(0)}}{\partial t} + c_{ki\alpha}\frac{\partial f_{ki}^{(0)}}{\partial r_\alpha} + \left(1 - \frac{1}{2\tau}\right)\left(\frac{\partial f_{ki}^{\mathrm{neq}}}{\partial t} + c_{ki\alpha}\frac{\partial f_{ki}^{\mathrm{neq}}}{\partial r_\alpha}\right) = -\frac{1}{\tau\delta t}f_{ki}^{\mathrm{neq}} \tag{17}$$

Performing summation on Equation (16) and using Equation (12), the following continuous equation can be obtained:

$$\frac{\partial \rho}{\partial t} + \frac{\partial(\rho u_\alpha)}{\partial r_\alpha} = 0 \tag{18}$$

Similarly, multiplying the particle velocity $c_{ki\alpha}$ with Equation (17), and then performing summation on it making use of Equations (12) and (16), the momentum equation is obtained as

$$\rho\frac{\partial u_\alpha}{\partial t}+\rho u_\beta\frac{\partial u_\alpha}{\partial r_\beta}=-\frac{\partial P}{\partial r_\alpha}+\frac{\partial F_\mu}{\partial r_\alpha} \tag{19}$$

in which

$$F_\mu=v\frac{\partial\rho u_\alpha}{\partial r_\beta}+\delta t\left(\tau-\frac{1}{2}\right)\frac{\partial P}{\partial t}+\delta t\left(\tau-\frac{1}{2}\right)\frac{\partial\rho u_\alpha u_\beta}{\partial t}$$

$$v=\frac{2e\delta t}{D}\left(\tau-\frac{1}{2}\right)$$

where v is the coefficient of kinematical viscosity and F_μ is viscous stress. Compared with the Navier–Stokes viscous transport term, the viscous stress F_μ in Equation (19) has extra unsteady pressure and momentum flux terms. The unsteady term may be neglected for small Mach numbers but the momentum flux term must be retained.

Multiply Equation (17) with the particle velocity c_k^2 and perform summation, and get the following energy equation:

$$\frac{\partial}{\partial t}\left(\frac{1}{2}\rho u_\alpha^2+\rho e\right)+\frac{\partial}{\partial r_\alpha}\left(\left(\frac{1}{2}\rho u_\alpha^2+\rho e+P\right)u_\alpha\right)=\frac{D+2}{D}\,\delta t\rho e\left(\tau-\frac{1}{2}\right)\frac{\partial^2 e}{\partial r_\alpha^2}+O(\varepsilon^3) \tag{20}$$

where thermal diffusion coefficient

$$\kappa=\frac{D+2}{D}\,\delta t\rho e\left(\tau-\frac{1}{2}\right)$$

4. NUMERICAL EXPERIMENT

In this numerical experiment, we intend to investigate and compare the stability properties and applicability of the lattice Boltzmann models described above. The example chosen is a standard test case concerning with the reflections of shockwaves on the surface of a triangular obstacle [9]. Figure 2 presents two sketches for flow field computation. The numbers in the diagram indicate the numbers of discrete lattice on each side of the obstacle. The zone covered by 250×1040 grids on the left-hand side of Figure 2(a) is the high-pressure area. The initial conditions are set as $(\rho_L,u_\alpha,e_{\mathrm{L}})=(25.0,0.0,0.40)$. The rest is the low-pressure area, and the initial conditions are set as $(\rho_R,u_\alpha,e_{\mathrm{R}})=(12.0,0.0,0.40)$. The relaxation time coefficient is taken as $\tau=0.6$. Non-slip bounce-back boundary conditions [13] are imposed on the four-side circumference boundaries, and on the sloping side in the bottom part. Figure 3(a) gives the numerical result obtained using the D2Q13 model with the integration time being 650. The propagation of shockwaves and their reflections on the sloping plane can be clearly seen in Figure 3. The predicted density contours are also consistent with those from the experiment [9]. Figure 2(b) gives the conditions for the second flow field computation. Now the high-pressure area on the left-hand side of the diagram is covered by 200×500 grid and the initial conditions

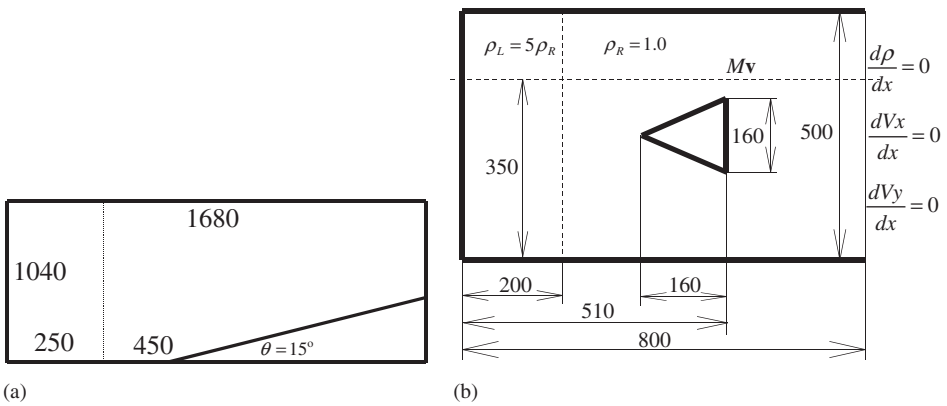

Figure 2. Structural illustration for flow field computation.

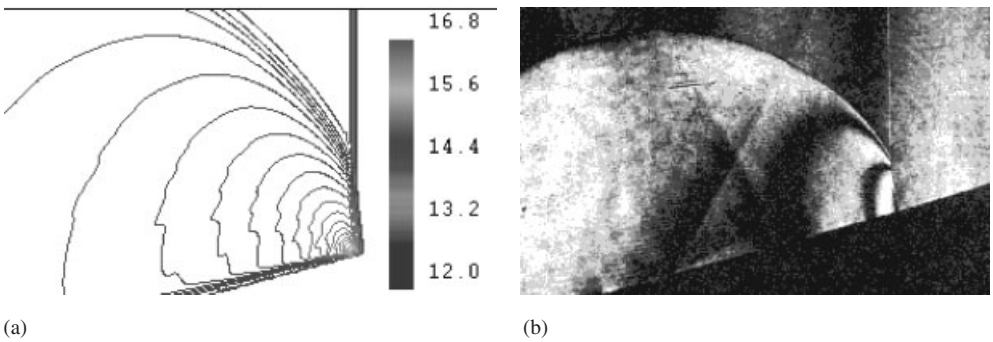

Figure 3. (a) Calculated density contours using D2Q13 (values ranging from 14 away from the tip to 16 near the tip). (b) Experimental observation [9].

there are set as $(\rho_{\mathrm{L}}, u_\alpha, e_{\mathrm{L}}) = (3.0\rho_{\mathrm{R}}, 0.0, 0.65)$. The rest is the low-pressure area where the initial conditions are set as $(\rho_{\mathrm{R}}, u_\alpha, e_{\mathrm{R}}) = (1.0, 0.0, 0.65)$. The relaxation time coefficient is taken as $\tau = 0.6$. Non-slip bounce-back boundary conditions are again implemented for the solid and side boundaries while on the right-hand side open boundary the zero gradient conditions are imposed as

$$\frac{\mathrm{d}\rho}{\mathrm{d}x} = 0, \quad \frac{\mathrm{d}Vx}{\mathrm{d}x} = 0, \quad \frac{\mathrm{d}Vy}{\mathrm{d}x} = 0$$

Figure 4 shows the computation result with the D2Q19 model for the shockwave reflections, and it has clearly demonstrated the propagation of shockwaves and their reflections on the folded angle. The numerical result is also consistent with experiment result [9]. Figure 5(a) shows the pressure distribution of flow field along x-axis at the dashed line positions $M\mathbf{v}$ of Figure 2(b). The property of rarefaction wave propagation and contact discontinuity can be seen clearly in the diagram. Figure 5(b) shows the velocity distribution of flow field along the same line. The abrupt jump of velocity on the sloping plane of the triangle, a phenomenon occurring also at the contraction section of Laval nozzle, is predicted. This abrupt jump of

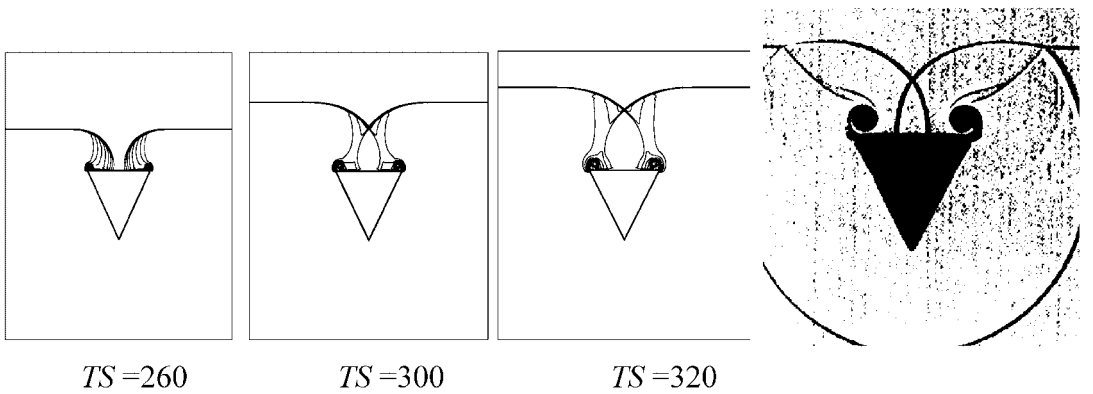

Figure 4. Comparison of the computation result of D2Q19 model for shockwave reflections with experiment result [9], where TS is the integration time step. The solid lines in the figure are the pressure distribution.

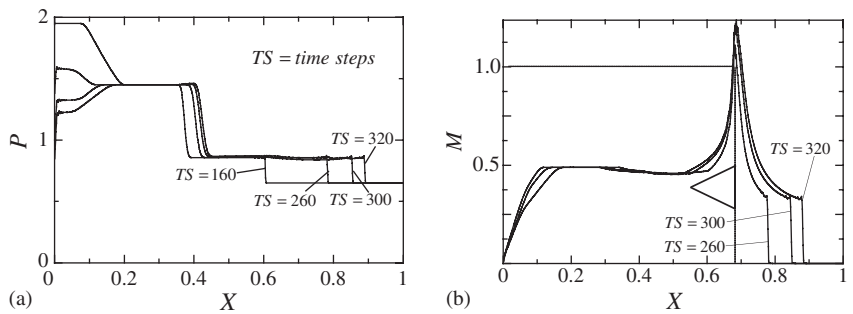

Figure 5. (a) Pressure distribution. (b) The distribution of Mach-number $M = Vx/a$ of the flow field along the dashed line $M\mathbf{v}$ (Vx is the flow velocity along axis X, and a is sonic speed, and $a^2 = 2e/D$).

velocity can be easily explained by using the one-dimensional dynamic equation in a variable cross-section tunnel which is both isoentropic and steady:

$$(M^2 - 1)\frac{\mathrm{d}V}{V} = \frac{\mathrm{d}A}{A} \tag{21}$$

The equation shows that if $M^2 - 1 < 0$, i.e. $M < 1$ and the flow velocity is subsonic, $\mathrm{d}V/V$ and $\mathrm{d}A/A$ must have opposite signs. Therefore, the gradual decrease in cross-section will result in the gradual increase in gas flow velocity. At the location of folded angle, $\mathrm{d}A/A = 0$ and the flow velocity reaches the critical state, i.e. $M = 1$. An almost instantaneous rapid acceleration of the flow beyond the folded angle will take place before arriving at the supersonic status. Following this rapid acceleration, the flow enters the pipe with constant cross-section ($\mathrm{d}A/A = 0$) with $(M^2 - 1)\mathrm{d}V/V < 0$. This means that the terms $\mathrm{d}V/V$ and $M^2 - 1$ are always of the opposite signs, resulting in the gradually attenuation of the supersonic flow.

Figure 6 shows that the relationship between the contact discontinuity of wave front and the dimensionless relaxation time τ. With the increase of the relaxation time τ, the contact discontinuity is seen to move from strong to weak.

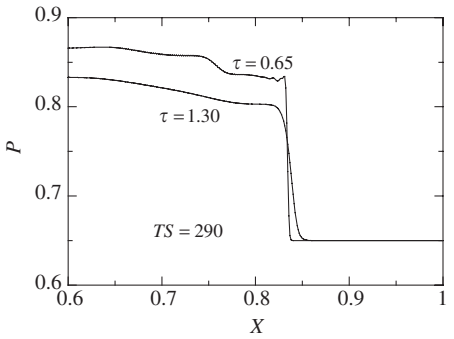

Figure 6. Pressure distributions for the integration time steps 290, the dimensionless relaxation times $\tau = 0.65$ and 1.30.

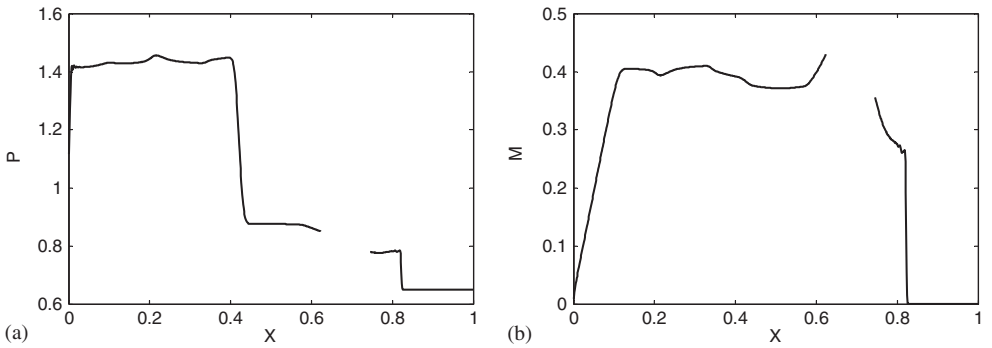

Figure 7. (a) and (b) show the distributions of pressure and the Mach-number, respectively, for the integration time steps 290.

As the equilibrium distribution is given by a truncated power series in the local fluid velocity, numerical accuracy and stability of LB model will be affected by the truncated error of the equilibrium distribution. The second numerical example is implemented with the same initial and boundary conditions by using the equilibrium distribution of second order in velocity **u**:

$$f_{ki}^{(0)} = W_k \rho (1 - 2Ec_{ki\alpha}u_\alpha + 2E^2 c_{ki\alpha}c_{ki\beta}u_\alpha u_\beta + Eu^2)$$

The numerical results (Figure 7) for the integration time steps 275 appears non-stability and overflow error of floating point of computing data at turning corner. The breaking section of distribution of pressure and Mach number is the region of overflow error of floating point as shown in Figure 7. Using same computing conditions, the equilibrium distribution of third order in **u** for D2Q19 model can give good numerical results as shown in Figure 5.

5. CONCLUSION

The two-dimensional D2Q13 and D2Q19 lattice Boltzmann models are established in this study by relationship criteria between the microscopic particle populations and macroscopic fluid. Macroscopic fluid dynamic equations can be derived from the models. The numerical stability and accuracy are guaranteed further by using the equilibrium distribution of third order in **u**. The good results have been got from the numerical simulation of the reflection phenomena of shockwaves on the surface of obstacles with this model. Thus the applicability of the lattice Boltzmann model is verified in both theory and experiment.

ACKNOWLEDGEMENTS

This research is partially supported by the UK Engineering and Physical Sciences Research Council through a research grant (GR/R72532/01) and by the National Natural Science Foundation of China (Grant Nos. ZKCX2-SW-210, and 8-1502). The authors would also like to thank the anonymous referees whose comments and suggestions have helped to improve the paper.

REFERENCES

1. McNamara G, Zanetti G. Use of the Boltzmann equation to simulate lattice-gas automata. *Physical Review Letters* 1988; **61**:2332–2335.
2. McNamara G, Alder B. Analysis of the lattice boltzmann treatment of hydrodynamics. *Physica A* 1993; **194**: 218–228.
3. Chen H, Chen S, Matthaeus WH. Recovery of the Navier–Stokes equations using a lattice-gas Boltzmann method. *Physical Review A* 1992; **45**:5339–5342.
4. Bhatnagar PL, Gross EP, Krook M. A model for collision processes in gases. I. Small amplitude processes in charged and natural one-component systems. *Physical Review* 1954; **94**:511–525.
5. Rothman DH, Zaleskl S. *Lattice-Gas Cellar Automata*. Cambridge University Press: London, 1996.
6. Chen S, Chen H, Martinez D, Matthaeus WH. Lattice Boltzmann model for simulation of magneto-hydrodynamics. *Physical Review Letters* 1991; **67**:3776–3779.
7. Succi S, Benzi R, Higuera F. The lattice Boltzmann-equation—a new tool for computational fluid-dynamics. *Physica D* 1991; **47**:219–230.
8. Chen S, Wang Z, Shan X, Doolen GD. Lattice Boltzmann computational fluid-dynamics in 3 dimensions. *Journal of Statistical Physics* 1992; **68**:379–400.
9. Dyke MV. *An Album of Fluid Motion*. Stanford Univ Press: Fourth Printing, 1988.
10. Alexander FJ, Chen S, and Sterling D. Lattice Boltzmann thermohydrodynamics. *Physical Review E* 1993; **47**:2249–2252.
11. Frisch U, d'Humières D, Hasslacher B, Lallemand P, Pomeau Y, Rivet JP. Lattice gas hydrodynamics in two and three dimensions. *Complex Systems* 1987; **1**:649–707.
12. Feng SD, Tsutahara M. Some progress in the lattice Boltzmann model. *Chinese Physics* 2001; **10**:587–593.
13. Ziegler DP. Boundary-conditions for lattice Boltzmann simulations. *Journal of Statistical Physics* 1993; **71**:1171–1177.

